Implementation and calibration of finite-length plastic hinge elements for use in seismic structural collapse analysis

Filipe L.A. Ribeiro [1], Luis A.C. Neves [2], Andre R. Barbosa [3]

ABSTRACT

Finite-length plastic hinge (FLPH) models have shown advantages over the concentrated plasticity hinge (CPH) models. However, empirical phenomenological relationships, such as Modified Ibarra-Medina-Krawinkler (ModIMK) deterioration model, were mainly calibrated for use in CPH models. ModIMK relationships are versatile and have been applied to steel, reinforced concrete, and timber structures. Herein, a calibration procedure of FLPH models and a unified algorithm for use of ModIMK relationships in CPH and FLPH models are presented. Results from included examples validate the proposed algorithms, which were implemented in OpenSees. Additionally, results highlight that FPLH models avoid errors and convergence pitfalls of CPH models.

Keywords: calibration, collapse, deterioration, finite elements, finite-length plastic hinge, concentrated plasticity, frame models, seismic analysis.

INTRODUCTION

Accurately modeling the behavior of structural members under large cyclic deformations is paramount for the quantification of the seismic performance of structures with some degree of confidence. The behavior of structural elements under these extreme loading conditions is

[1]Ph.D. Student, UNIC, Department of Civil Engineering, Faculdade de Ciências e Tecnologia - Universidade Nova de Lisboa, Quinta da Torre, 2829-516 Caparica, Portugal. Visiting Ph.D. Student, School of Civil and Construction Engineering, Oregon State University, Corvallis, OR 97331-3212, USA, E-mail: f.ribeiro@fct.unl.pt

[2]Lecturer, Nottingham Transport Engineering Centre (NTEC), University of Nottingham, University Park, Nottingham, NG7 2RD, UK. UNIC, Department of Civil Engineering, Faculdade de Ciências e Tecnologia - Universidade Nova de Lisboa, Quinta da Torre, 2829-516 Caparica, Portugal, E-mail: luis.neves@nottingham.ac.uk

[3]Assistant Professor, School of Civil and Construction Engineering, Oregon State University, 101 Kearney Hall, Corvallis, OR 97331-3212, USA, E-mail: andre.barbosa@oregonstate.edu

extremely complex. Thus, several simulation approaches have been proposed which include models of varying complexity and computational cost. Continuum models are generally considered as the most reliable approach for estimating the seismic demands of structures to localized and global collapse, but they are typically complex and lead to extensive computational effort.

Concentrated plasticity hinge (CPH) elements are used herein as a reference modelling approach, considering the vast experience on the use of these in the modeling of buildings under seismic loads (Ibarra and Krawinkler, 2005; Medina and Krawinkler, 2005; Haselton and Deierlein, 2007; PEER/ATC, 2010). In these models, each structural element is modeled as the association of a linear elastic beam element and a nonlinear spring at each member modified. The correct linear-elastic solution for the entire member is only obtained if the end rotational springs are approximated as rigid-plastic. This is usually achieved using an ad-hoc stiffness modifier parameter, n_{Factor}, for the zero-length springs. However, the definition of the ideal value n_{Factor} is not trivial, as a low value leads to erroneous results and a high value results in numerical instability and convergence issues. As discussed in detail in this work, the use of n_{Factor} also increases significantly the complexity of the implementation of nonlinear constitutive models. If a CPH model is used in the development of a structural model, moment-rotation relationships directly obtained from experimental tests can be employed to define the nonlinear zero-length springs that control element flexural response. Distributed plasticity models (Spacone et al., 1996; Neuenhofer and Filippou, 1997) have also been widely used in the development of numerical models and have been implemented in finite element softwares. Based on this formulation of distributed plasticity, alternative approaches have been proposed by different authors to limit the effects of localization phenomena related to non-objective strain-softening response of distributed plasticity force-based beam-column elements (Coleman and Spacone, 2001). Force-based finite-length plastic hinge (FLPH) beam-column elements were developed by Scott and Fenves (2006) and Addessi and Ciampi (2007) as an alternate formulation to address localization issues.

The FLPH elements include two discrete length plastic hinge zones at element ends and a linear elastic region in between the hinge zones, all of which are incorporated through an appropriate element numerical integration scheme. When compared to the CPH approach, this model has been shown to be advantageous, namely in what concerns to modeling effort, computational cost, clear separation between member and connection nonlinearity, and more realistic modelling of yielding progression and hinge rotations. When empirically calibrated moment-rotation models are used to define the inelastic FLPH elements, a calibration procedure is needed. This was first identified by Scott and Ryan (2013) and a solution was proposed by Ribeiro et al. (2014) for sections exhibiting softening response under monotonic loading. Combined with empirically calibrated constitutive relationships, these models allow for reliable estimation of the seismic structural demands up to the onset of collapse with limited computational cost.

Many hysteric laws have been proposed in the last decades to model the performance of different structural elements and structural materials subjected to large cyclic displacements. The main observed nonlinear phenomena include cyclic deterioration in stiffness (Takeda et al., 1970) and strength (Pincheira et al., 1999; Sivaselvan and Reinhorn, 2000), and pinching under load reversal (Roufaiel and Meyer, 1987). Among these models, the Modified Ibarra-Medina-Krawinkler (Lignos, 2008), denoted ModIMK, was selected herein for its versatility. The ModIMK model has been applied to RC (Haselton and Deierlein, 2007), steel (Lignos and Krawinkler, 2011), and timber structures (Ibarra and Krawinkler, 2005). Since these models were mainly developed to describe force-displacement (e.g. moment-rotation) relations for use in concentrated hinges, their use in FLPH elements requires modifications, alternative implementation, and special calibration considerations. In fact, as shown in Scott and Ryan (2013) and Ribeiro et al. (2014), the use of simple scaling of the constitutive law by the plastic hinge length to define a moment-curvature relation in FLPH models leads to inconsistent pushover results.

The main objective of this paper is to present a unified implementation algorithm of the ModIMK deterioration models for use in CPH and FLPH models. For the CPH model, new implementations are provided for updating the unloading stiffness and the post-yield hardening ratio, as well as, the computation of the committed member displacements and the updated spring displacements. For the FLPH models, an extended calibration procedure is proposed, which updates the flexural stiffness of the interior sections of the member to provide objective and consistent element responses when empirically calibrated moment rotations rules are employed for cyclic analysis. The formulation and implementation proposed was included in a modified version of the Open System for Earthquake Engineering Simulation (OpenSees, Mazzoni et al. (2009) 2.4.3, r5695) framework. Results from included examples validate the proposed algorithms. Additionally, results highlight that FPLH models avoid errors and convergence pitfalls of CPH models.

BACKGROUND

Concentrated Plasticity Hinge Models

In CPH models, two discrete zero-length hinges are defined at member ends and a linear elastic region is defined in-between the two zero-length hinges. These three components are associated in series to define a CPH member. The flexibility matrix of this member, $\mathbf{f_{mem}}$, is given by:

$$\mathbf{f_{mem}} = \mathbf{f_{sI}} + \mathbf{f_{int}} + \mathbf{f_{sJ}} \tag{1}$$

where $\mathbf{f_{int}}$ is the flexibility of the linear-elastic interior element and $\mathbf{f_{sI}}$ and $\mathbf{f_{sJ}}$ are the flexibilities of the springs at ends I and J, respectively. The elastic stiffness of the member is given as the inverse of the flexibility matrix shown in Equation 1. The model stiffness is therefore related to the elastic stiffness of the rotational springs and the beam-column element, which are connected in series. When a CPH model is used to model an elastic beam-column member, the correct linear-elastic solution for the entire model is only obtained if rigid-plastic zero-length end springs are defined. Thus, the linear elastic stiffness of the springs at both ends are amplified by a constant factor n_{Factor} such that the initial stiffness of the springs is large, but not so large as to pose numerical instability. During the nonlinear analysis, the n_{Factor} must be considered when the stiffness of the element is computed (e.g., when updating the post-yield stiffness).

Finite-length Plastic-hinge Models

The use of finite-length plastic-hinge (FLPH) models in nonlinear analysis requires the definition of one single element in which inelastic hinge zones with discrete length are defined at element ends. The FLPH elements (Scott and Fenves, 2006; Addessi and Ciampi, 2007) are based on force-based distributed plasticity formulations in which the element integration is performed using methods that allow for the definition of a user defined hinge length at element ends.

In this model both end sections are assigned a nonlinear behavior, whereas the element interior is typically assumed to have an elastic behavior, however this assumption is not necessary. The flexibility of the FLPH element is computed as:

$$\mathbf{f} = \int_{L_{pI}} \mathbf{b}(x)^T \mathbf{f_S}(x) \mathbf{b}(x) dx + \int_{L_{int}} \mathbf{b}(x)^T \mathbf{f_S}(x) \mathbf{b}(x) dx + \int_{L_{pJ}} \mathbf{b}(x)^T \mathbf{f_S}(x) \mathbf{b}(x) dx \qquad (2)$$

where L_{pI} and L_{pJ} are the length of the plastic hinges at element ends, L_{int} is the length of the linear-elastic element interior, $\mathbf{b}(x)$ is the interpolation function matrix, and $\mathbf{f_S}$ is the section flexibility, nonlinear for the first and third term, and typically linear for the second term. For other formulation details see Scott and Fenves (2006), for example.

CONSTITUTIVE LAWS FOR CYCLIC LOADING

In this paper, the modified Ibarra-Medina-Krawinkler deterioration model (Lignos, 2008), ModIMK model in short, was chosen for its versatility in modeling degrading hysteretic response of structural elements. This model was empirically calibrated for reproducing the moment-rotation relation of reinforced concrete (Haselton and Deierlein, 2007) and steel structural components (Lignos and Krawinkler, 2011). The ModIMK model is based on: (i) a backbone curve defining the reference monotonic behavior, (ii) a set of rules defining the hysteretic behavior between the positive and negative backbone curves; and (iii) a set of rules that define up to six modes of deterioration of the hysteretic behavior.

Figure 1(a) illustrates the parameters that define the backbone curve. This curve is defined by three strength parameters: effective yield strength (or basic strength), F_y, capping strength, F_C (or post-yield strength hardening ratio F_C/F_y), and residual strength, F_r; and four deformation parameters: yield deformation, d_y, pre-capping plastic deformation for monotonic loading, d_p, post-capping plastic deformation, d_{pc}, and ultimate deformation capacity, d_u. The ModIMK model defines six modes of cyclic strength and stiffness deterioration: (i) basic strength, (ii) post-yield hardening ratio, (iii) post-capping strength, (iv) unloading stiffness, (v) reloading stiffness, and (vi) pinching behavior. Figures 1(b) to 1(d) illustrate three models that have been proposed in the literature based on different combinations of these six modes of deterioration. All three models share the same backbone curve. The models are:

- Bilinear hysteretic response (Bilin) model with strength deterioration (Figure 1b);
- Peak-oriented model with strength and stiffness deterioration (Figure 1c);
- Pinching model with strength and stiffness deterioration (Figure 1d).

In the ModIMK models, the rates of cyclic deterioration are controlled by a characteristic total hysteretic energy dissipation capacity E_t and an energy based rule developed in Rahnama and Krawinkler (1993). The characteristic total hysteretic energy dissipation capacity E_t is obtained from experimental results.

The energy based rule developed by Rahnama and Krawinkler (1993) expresses the cyclic deterioration in excursion i, β_i:

$$\beta_i = \left(\frac{E_i}{E_t - \sum_{j=1}^{i} E_j} \right)^c \leq 1 \tag{3}$$

where E_i is the hysteretic energy dissipated in excursion i, and $\sum E_j \leq E_t$ is the hysteretic energy dissipated in all previous excursions in both positive and negative directions. The exponent c defines the rate of deterioration. According to Rahnama and Krawinkler (1993), a reasonable range of values for c is between 1.0 and 2.0. β_i ranges between 0 and 1.

The generalized stiffness or strength parameter, X, can be updated through:

$$X_i = (1 - \beta_k) \times X_{i-1} \tag{4}$$

where X_i is the value of the parameter in excursion i and β_k is the value of deterioration parameter.

The ModIMK is used herein to model the behavior of plastic hinges. However, the implementation of this model within a finite element framework is complex and dependent on the type of finite element used. In the following sections the details regarding a consistent and unified implementation of these models is provided for CPH and FLPH models.

IMPLEMENTATION OF MODIMK MODELS IN HINGE ELEMENTS

Figure 2 shows the general procedure used to update the ModIMK model parameters. This procedure is a direct application of the proposal by Ibarra et al. (2005), and it is detailed here for completeness of the discussion on new implementation that follows in the next subsections. At the beginning of the analysis, the model parameters are initialized. In the elastic range, no change in these parameters occurs and no update of the constitutive law is required. The unloading stiffness is the only parameter which is updated when a load reversal takes place in the inelastic range. In a finite element implementation, the stiffness must be known before the reversal, requiring the updating of the unloading stiffness in all steps in the inelastic range. Furthermore, this is the only deterioration mode for which a common deterioration parameter is used in both loading directions.

The remaining parameters are updated at the end of the unloading branch ($F_{n-1} \times F_n < 0$), denoted by point Y in Figure 1. At this point, dissipated energy in the previous excursion is computed. This allows for updating of the reloading stiffness, the basic strength, the strain hardening ratio, the capping point, and the pinching parameters for the current excursion. The procedure is then repeated for each excursion reaching the nonlinear range.

Implementation in Concentrated Plastic Hinge Models

In the CPH model, to guarantee the rigid plastic behavior of the springs, their initial stiffness is given by:

$$k_{s,m} = (n_{Factor} + 1) \times K_{mem}, \qquad m = I, J \tag{5}$$

where K_{mem} is the elastic stiffness of the member. In the case of double curvature, $K_{mem} = 6EI/L$, where EI the is cross-section flexural stiffness, and L is the member length. Since the elastic stiffness of the member is related to the elastic stiffness of the rotational springs and the interior elastic element, which are connected in series, the stiffness of the interior element, k_{int}, is also affected by n_{Factor}, as:

$$k_{int} = \frac{n_{Factor} + 1}{n_{Factor}} \times K_{mem} = \frac{6EI_{mod}}{L} \tag{6}$$

where $EI_{mod} = \frac{n_{Factor}+1}{n_{Factor}} EI$ is the modified elastic stiffness of the element interior.

In the post-yielding region, member stiffness is computed by multiplying the elastic stiffness by the post-yielding ratio, α. Since the elastic stiffness of the zero-length spring is affected by the n_{Factor}, an adjusted post-yielding ratio of the spring, α' (ratio of the tangent stiffness, k_{Ts}, to the linear elastic stiffness, k_s) is given by:

$$\alpha' = \frac{k_{Ts}}{k_s} = \frac{\alpha}{1 + n_{Factor} \times (1 - \alpha)} \tag{7}$$

The introduction of an n_{Factor} in the definition of the zero-length springs requires that several modifications are considered in the ModIMK implementation and general deterioration model given in Equation 4. The adjusted implementation details when defining moment-rotation empirical relations in CPH models are presented next for each of the six deterioration modes. For comparison purposes, a simplified implementation, where the effect of n_{Factor} is not considered in the updating of model parameters, is denoted as CPH-original. In general, two main adjustments are made. First, the stiffness of the nonlinear spring is updated so that the stiffness of the entire element is equal to the objective stiffness. Second, the displacements of the springs need to be updated so that the correct target displacements (rotations) of the element are achieved. In what regards strengths, since the force (moment) in the spring is equal to the force (moment) in the element ends, no adjustment is required. Therefore, the basic and post-capping strength deterioration follows the general form of Equation 4.

The zero-length spring stiffness is affected by the n_{Factor} and the post-yielding ratio of the spring defined in Equation 7 is used. When computing the deterioration of the post-yielding hardening ratio the general model described in Equation 4 is not applicable. Instead, the deterioration of the post-yielding hardening ratio is computed using the new procedure shown in Figure 3. In this procedure, first, the member hardening ratio of the previous excursion is computed using the inverse of Equation 7. Second, given β_i, the member post-yielding stiffness is updated. Lastly, Equation 7 is used to compute the updated hardening ratio of the nonlinear springs.

Since the unloading stiffness deterioration depends on the energy dissipated up to the beginning of the unloading branch rather than that dissipated in a complete excursion, an implementation different than the one proposed by Ibarra and Krawinkler (2005) is used herein for this parameter. Equation 4 is thus replaced by:

$$K_{u,n}^{member} = \left[\prod_{j=1}^{i-1}(1-\beta_{k,j})\right] \times (1-\beta_{k,n}) \times K_0 = \gamma_k \times K_0 \tag{8}$$

where i is the total number of inelastic excursions up to load step n, $\beta_{k,j}$ is the deterioration parameter associated with completed inelastic excursion j, $\beta_{k,n}$ is the deterioration parameter computed considering the energy dissipated in excursion i up to load step n, γ_k is the cumulative deterioration of the unloading stiffness and K_0 is the member initial elastic stiffness. The procedure starts by computing the residual energy dissipation capacity, $E_t - \sum E_j$

and the damage parameter β_k. Equation 8 is then used to update the unloading stiffness of the element based on its elastic stiffness. The unloading spring stiffness is thus given by:

$$K_{u,n}^{spring} = \left(\frac{\gamma_k}{1 + n_{Factor} \times (1 - \gamma_k)} \right) \times K_0 \tag{9}$$

where K_0 and $K_{u,n}^{spring}$ are the original member elastic stiffness and updated unloading stiffness of the zero-length spring in loading step n.

The reloading stiffness deterioration is modeled by increasing the absolute value of the target displacement of the member, d_i, corresponding to the horizontal coordinate of point Y in Figure 1c, in each direction as:

$$d_i = (1 + \beta_i) \times d_{i-1}^{max} \tag{10}$$

where d_{i-1}^{max} is the maximum displacement observed up to the $i - 1$ excursion in the same direction.

The implemented algorithm for computing the reloading stiffness deterioration in CPH models is presented in Figure 4. Firstly, the maximum displacement of the member in previous excursions, $d_{i-1}^{max,member}$, is computed using the general relation between spring and member rotations:

$$d^{spring} = d^{member} - d^{elastic} = d^{member} - F(d^{member}) \times K_{member} \tag{11}$$

where $F(d^{member})$ is the force associated with the displacement d^{member}, obtained with the backbone curve computed for the current step of the analysis. $F(d^{member}) \times K_{member}$ is thus the elastic deformation of the member, associated with the force $F(d^{member})$ under the assumption of double curvature.

The updated member maximum displacement is then updated using Equation 10. Then, the updated backbone curve for this excursion is defined, based on the updated basic strength, post-yielding ratio, and post-capping strength. This is then used to compute the force $F(d_i^{max,member})$. The maximum deformation of the zero-length spring can then be calculated using Equation 11.

Finally, the reloading stiffness is defined using point Y in Figure 1 and the new maximum deformation point ($d_i^{max,spring}$; $F^i(d_i^{max,member})$). The maximum deformation is monitored in each load step.

The implementation of updates of the pinching parameters is similar to that described for the reloading stiffness. The additional notable point in reloading (see point P in Figure 1d) is computed by multiplying the yielding displacement and the corresponding force by parameters A_{pinch} and $F_p^{\pm}$, respectively. Firstly, the maximum deformation in the member is calculated, using the relationship presented in Equation 11. Then, the intermediate point for pinching response is computed for the member by multiplying factors A_{pinch} and $F_p^{\pm}$ (for positive loading direction) to the maximum deformation and associated force, respectively. Once this intermediate point is found, the corresponding intermediate point for the zero-length spring is computed using Equation 11. Finally, the stiffness associated with the two branches that characterize pinching response can be computed for the CPH member.

Implementation and Calibration in Finite-length Plastic-hinge Models

If the deteriorating models described herein are applied to $FPLH$ elements, the implementations developed by Ibarra and Krawinkler (2005) do not require modifications, as the objective stiffness and displacements can be directly assigned to the member. This results in a much simpler implementation based on the general algorithm presented in Figure 2 and the general updating Equation (Eq. 4). This is one of the main advantages of using FLPH models, i.e. that the original hysteretic laws do not need adjustments as is the case when CPH models are used.

As shown by Scott and Ryan (2013), employing a moment-rotation constitutive law dividing the rotations by the plastic hinge length to obtain a moment-curvature relation produces inconsistent results and the objective moment-rotation response is not recovered. Thus, Scott and Ryan (2013) proposed a calibration procedure to address this issue. However, the calibration procedure was developed for hardening responses only. An alternate calibration procedure developed by Ribeiro et al. (2014) was proposed for both hardening and softening responses under monotonic loading. This procedure is extended here for cyclic loading.

The detailed formulation of the FLPH elements is presented in Scott and Fenves (2006). In the interest of brevity, only a description of key aspects is presented here. The member flexibility using the modified Gauss-Radau integration scheme is given by:

$$\mathbf{f} = \sum_{i=1}^{N_{pI}} (\mathbf{b}^T \mathbf{f}_s \mathbf{b}|_{x=\xi_i}) w_i + \int_{L_{int}} \mathbf{b}(x)^T \mathbf{f}_S(x) \mathbf{b}(x) dx + \sum_{i=N_{pI}+1}^{N_{pI}+N_{pJ}} (\mathbf{b}^T \mathbf{f}_s \mathbf{b}|_{x=\xi_i}) w_i \tag{12}$$

where N_{pI} and N_{pJ} are the number of integration points associated with the plastic hinges at the element ends, and $\mathbf{f_s}(x)$ is the section flexibility. For the modified Gauss-Radau integration $N_{pI} = N_{pJ} = 2$. The interior element term (middle term in the right hand side of Equation 12) can be computed analytically or numerically. In the latter case, the Gauss-Legendre integration scheme can be used. If two integration points are placed in this region, a total of six integration points are defined along the member length. The location ξ_i of the integration points associated with the modified Gauss-Radau plastic hinge integration is given by:

$$\xi = \{\xi_\mathbf{I}, \xi_\mathbf{int}, \xi_\mathbf{J}\} \tag{13}$$

where:

$$\begin{gathered} \xi_\mathbf{I} = \left\{0; \tfrac{8L_{pI}}{3}\right\} \\ \xi_\mathbf{int} = \left\{4L_p + \tfrac{L_{int}}{2} \times \left(1 - \tfrac{1}{\sqrt{3}}\right); 4L_p + \tfrac{L_{int}}{2} \times \left(1 + \tfrac{1}{\sqrt{3}}\right)\right\} \\ \xi_\mathbf{J} = \left\{L - \tfrac{8L_{pJ}}{3}; L\right\} \end{gathered} \tag{14}$$

The corresponding weights w_i are given by:

$$\mathbf{w} = \{\mathbf{w_I}, \mathbf{w_{int}}, \mathbf{w_J}\} \tag{15}$$

where:

$$\mathbf{w_I} = \{L_{pI}; 3L_{pI}\} \;\; \mathbf{w_{int}} = \left\{\tfrac{L_{int}}{2}; \tfrac{L_{int}}{2}\right\} \;\; \mathbf{w_J} = \{3L_{pJ}; L_{pJ}\} \tag{16}$$

In this case, the element flexibility is then given by:

$$\mathbf{f} = \sum_{i=1}^{6} (\mathbf{b}^T \mathbf{f}_s \mathbf{b}|_{x=\xi_i}) w_i \tag{17}$$

The inclusion of experimentally calibrated moment-rotation relations to define the behavior of nonlinear regions can be implemented by modifying the flexural stiffness at integration points in the elastic region of the FLPH member (see Figure 5), so that the flexibility matrix of the calibrated FLPH member is equal to a reference flexibility, which is considered as that of the CPH model with $n_{Factor} \to \infty$. In a 2D beam-column element, a system of three integral equations corresponding to each of the unique flexural coefficients of the element flexibility matrix is defined. The flexibility matrix of the FLPH element is computed using Equation 17, where

$$\mathbf{b} = \begin{bmatrix} x/L - 1 & x/L \end{bmatrix} \tag{18}$$

and

$$\{f_s(\xi_1); \cdots; f_s(\xi_6)\}^T = 1/EI \cdot \{\alpha_1 \times 6 \times L_{PI}/L; \beta_1; \beta_2; \beta_2; \beta_3; \alpha_2 \times 6 \times L_{PJ}/L\}^T \tag{19}$$

where α_1 and α_2 are the ratio between the nonlinear stiffness and the elastic stiffness at end I and J, respectively, and β_1, β_2 and β_3 are the flexural modification parameters.

The equivalent flexibility matrix, considering the CPH model is given by:

$$\mathbf{f_b} = \lim_{n_{Factor} \to \infty} \left\{ \begin{bmatrix} 1/k_{TI} & 0 \\ 0 & 0 \end{bmatrix} + \frac{L}{6EI_{mod}} \times \begin{bmatrix} 2 & -1 \\ -1 & 2 \end{bmatrix} + \begin{bmatrix} 0 & 0 \\ 0 & 1/k_{TJ} \end{bmatrix} \right\} \tag{20}$$

where $k_{TI} = (n_{Factor} + 1)\, K_{mem}$ and $k_{TJ} = (n_{Factor} + 1)\, K_{mem}$ are the tangent stiffness of the springs at ends I and J, respectively, and $EI_{mod} = \frac{n_{Factor}+1}{n_{Factor}} EI$.

From this system of equations, the three elastic stiffness modification parameters, β_1, β_2, and β_3, are computed as a function of L_{pI}, L_{pJ}, L and n_{Factor}. When the n_{Factor} tends to infinity, β_1, β_2 and β_3 are given by:

$$\begin{aligned}
\beta_1 &= -\frac{54L_{pI}L^3 - 6L_{pI}(60L_{pI}+60L_{pJ})L^2 + 6L_{pI}(96L_{pI}^2+288L_{pI}L_{pJ}+96L_{pJ}^2)L - 6L_{pI}(256L_{pI}^2L_{pJ}+256L_{pI}L_{pJ}^2)}{L(3L-16L_{pJ})(L^2-20LL_{pI}+4L_{pJ}L+64L_{pI}^2)} \\
\beta_2 &= -\frac{3(4L_{pI}-L+4L_{pJ})(3L^2-12LL_{pI}-12LL_{pJ}+32L_{pI}L_{pJ})}{L(3L-16L_{pI})(3L-16L_{pJ})} \\
\beta_3 &= -\frac{54L_{pJ}L^3 - 6L_{pJ}(60L_{pI}+60L_{pJ})L^2 + 6L_{pJ}(96L_{pI}^2+288L_{pI}L_{pJ}+96L_{pJ}^2)L - 6L_{pJ}(256L_{pI}^2L_{pJ}+256L_{pI}L_{pJ}^2)}{L(3L-16L_{pI})(L^2-20LL_{pJ}+4L_{pI}L+64L_{pJ}^2)}
\end{aligned} \tag{21}$$

Assuming both plastic hinges at member ends have similar lengths L_p, the stiffness modifying factors (β_1, β_2 and β_3, see Figure 5) are given by:

$$\begin{aligned}
\beta_1 &= \beta_3 = -\frac{6\left(3\,L^2\,L_p - 24\,L\,L_p^2 + 32\,L_p^3\right)}{L(L-8\,L_p)^2} \\
\beta_2 &= \frac{3\left(3\,L^3 - 48\,L^2\,L_p + 224\,L\,L_p^2 - 256\,L_p^3\right)}{L(3L-16\,L_p)^2}
\end{aligned} \tag{22}$$

As shown, these factors do not depend on the stiffness terms α_i, $\{i = 1, 2\}$ and therefore are constant during the analysis. Therefore Equation 22 only needs to be applied once at the beginning the analysis, implying a very limited computational cost. Moreover, this independence between the stiffness terms and the flexural modification factors makes this implementation independent of the constitutive law employed.

For the $FPLH$ model, in terms of calibration, the only other parameter that needs adjusting is the the total energy dissipation capacity E_t. This term is defined empirically for the moment-rotation relation, and can be defined, for moment-curvature, as:

$$E_t^{M-\chi} = E_t^{M-\theta}/L_p \tag{23}$$

All other parameters follow the general models developed and implemented by Ibarra and Krawinkler (2005).

NUMERICAL EXAMPLES

In this section a simple structure subjected to a set of cyclic pushover analyses is used to evaluate the accuracy and stability of the proposed implementations. The algorithms and procedures discussed were implemented in a modified version of the Open System for Earthquake Engineering Simulation (OpenSees, Mazzoni et al. (2009), 2.4.3, r5695) framework. In the examples, a simply supported beam subjected to different end moments (see Figures 6 to 10) is analyzed under cyclic displacement control considering the three material models discussed. The beam has a 24 feet ($7.33m$) span and the model parameters for all material models are presented in Table 1. The ultimate rotation, θ_u and the plastic hinge length, L_p, were taken equal to 0.4 rad and $L/16$, respectively, for all cases. For the Pinching model, three additional parameters that define the mid-point in the reloading branch are assumed to be equal to 0.4.

Figures 6, 7, and 8 shows results for analyses performed using the pinching model for moment gradients defined with one end moment, two anti-symmetric end moments, and two symmetrical end moments. The first set of results compares the results obtained using the CPH model, both considering direct application of Equation 4 (CPH-original) and using the proposed implementation (CPH-updated), with those obtained with the finite length plastic hinge model (FLPH) and an analytical solution. For the CPH-original, n_{Factor} was taken equal to 10 to reduce numerical instabilities, following recommendations in Ibarra and Krawinkler (2005) and Zareian and Medina (2010). For CPH-updated n_{Factor} was taken equal to 10 and 1000. Results show that all implementations lead to acceptable results. However, the CPH-original and CPH-updated, considering a n_{Factor} equal to 10, lead to a noticeable over-estimation of the elastic stiffness. This error propagates to the entire analysis, as can be seen at the end of the unloading branch. Moreover, as a result of not updating the stiffness of the elastic element interior during analysis, the CPH-original also leads to significant errors in the unloading and reloading stiffnesses. The analysis using the FLPH elements provide the results closest to the theoretical results, being clearly the most accurate model. Figures 6, 7, and 8 show that the amplitude of observed errors decrease with increase in the moment gradient along the element length, being smaller for the anti-symmetric loading and larger for the symmetric loadings. In addition, it is clear that the use of the CPH-original model does not allow for obtaining accurate results as the direct application of Equation 4, i.e. not considering the implementation procedures proposed herein, is not enough for correctly updating model parameters during the analysis. Figures 9 and 10, which show the results obtained for the Peak-oriented and Bilin models indicate that the conclusions drawn for the pinching model hold for the other material models.

In Figure 11 the errors in the elastic stiffness are plotted for the FLPH model and for the CPH-updated implementation with n_{Factor} values between 10 and 1000. Results show convergence of the error when the CPH-updated implementation is used. However, even for large $n_{factors}$ the CPH-updated produces the largest errors when estimating the elastic stiffness. It is clear that the FLPH model results in very small errors, only comparable with those obtained for the CPH-updated with an n_{Factor} equal to 1000. The results presented refer to the Bilin model, but conclusions hold for all constitutive models implemented.

To compare the numerical stability of different implementations, results of an elementary assessment are shown in Figure 12. The models were analysed considering the Krylov-Newton algorithm (Scott and Fenves, 2010) under displacement control analyses. Pseudo-time steps between 1×10^{-7} and 1×10^{-3} are used in the analyses. The norm of the displacement increment convergence test is used with a threshold of 1×10^{-8}. Figure 12 shows that FLPH and the CPH-original with n_{Factor} equal to 10 converged for all time steps. However, n_{Factor} values between 100 and 500 required a pseudo-time step smaller than 1×10^{-5} for achieving convergence. For a n_{Factor} equal to 1000, a pseudo-time step of 1×10^{-7} was necessary to achieve convergence. Although this is not an exhaustive convergence stability analysis, the results indicate that the FLPH is significantly more stable. Similar stability is obtained for the CPH-original model only if n_{Factor} is taken equal to 10 which, as shown above, leads to significant overestimation of the elastic stiffness.

CONCLUSIONS

Within the wide range of member models available in the literature, concentrated plasticity hinge (CPH) models have been the reference model for earthquake engineering studies during the last decade. However, finite-length plastic hinge (FLPH) models have been recently shown to be advantageous over the CPH models. A significant reduction in modelling effort, as well as in computational cost, a clear distinction between member and connection nonlinearities, and more realistic modelling of yielding progression and hinge rotations are the most important advantages of the FLPH model.

In this work, results obtained for cyclic analysis using implementation and calibration of the FLPH models are discussed and compared to those resulting from two implementations used for updating parameters of the unloading stiffness and other deterioration modes in the CPH models. All implementations were performed in the Open System for Earthquake Engineering Simulation (OpenSees) making use of the ModIMK material models, which have been widely used for simulating steel, RC, and timber frame structures.

In terms of the implementation, the main conclusions of this paper are:

1. a new unified implementation was developed in the OpenSees framework, where the ModIMK material models can now be used in both CPH and FLPH models;
2. the implementation of the ModIMK in the CPH models proved to be significantly more complex than that done for FLPH models. This results from the use, in this case, of three separate components, two zero-length springs and an elastic beam-column interior element. In addition, the elastic stiffness of the zero-length springs needs to be amplified in order to obtain the correct member flexibility matrix, which requires further adjustments in the updating procedure of all parameters of the springs;
3. in FLPH models, the main difficulty lies, not on the implementation of the ModIMK material models, but in the need to calibrate the element to consider empirical

moment-rotation relationships;

4. although a calibration procedure is required for the FLPH elements, this procedure can be used independently of the constitutive law. For the CPH models, custom implementations are required if different constitutive laws are to be used;
5. for FPLH models, once the formulation of the calibration is defined, the implementation procedure is significantly simpler and applicable to a wide range of constitutive deterioration models, thus not restricted to the ModIMK relationships;
6. the FLPH calibration proposed was validated for nonlinear cyclic analysis.

Based on the numerical results shown:

1. in general, CPH and FLPH models can provide reasonable results for nonlinear cyclic analysis;
2. for a beam element with anti-symmetric end moments, CPH models provide accurate results independently of the n_{Factor} that is used to amplify the elastic stiffness of the zero-length springs;
3. for a beam element with other moment gradients, non-negligible errors are obtained for the elastic stiffness if the n_{Factor} in CPH models is not large enough (e.g., approximately 5% error is obtained for symmetric bending moments for $n_{Factor} = 10$); these errors propagate throughout the analysis;
4. CPH models with large n_{Factor} values give rise to numerical instabilities;
5. calibrated FLPH models provided the most accurate results.

In summary, even though the use of FLPH models in large numerical studies requires more investigation, the results presented in this work indicate that these models are suitable for being used in large numerical simulations, being more stable, accurate, and versatile.

ACKNOWLEDGMENTS

The authors would like to acknowledge the support of the Portuguese National Science and Technology Foundation through the fellowship SFRH/BD/777722/2011 and grant

PTDC/ECM-COM/2911/2012. The first author would also like to acknowledge the support of Oregon State University during the period in which he was a visiting Ph.D. student. The third author would also like to acknowledge the support of Region X University Transportation Center (PacTrans) for providing partial funding in support of development of analytical tools for assessing the seismic performance of structures to collapse. The opinions and conclusions presented in this paper are those of the authors and do not necessarily reflect the views of the sponsoring organizations.

REFERENCES

Addessi, D. and Ciampi, V. (2007). "A regularized force-based beam element with a damage plastic section constitutive law." *International Journal for Numerical Methods in Engineering*, 70(5), 610–629.

Coleman, J. and Spacone, E. (2001). "Localization issues in force-based frame elements." *ASCE Journal of Structural Engineering*, 127(11), 1257–1265.

Haselton, C. and Deierlein, G. (2007). "Assessing seismic collapse safety of modern reinforced concrete frame buildings." *Report No. 156*, The John A. Blume Earthquake Engineering Center, Stanford University.

Ibarra, L. F. and Krawinkler, H. (2005). "Global collapse of frame structures under seismic excitations." *Report No. 152*, The John A. Blume Earthquake Engineering Research Center, Department of Civil Engineering, Stanford University, Stanford, CA.

Ibarra, L. F., Medina, R. A., and Krawinkler, H. (2005). "Hysteretic models that incorporate strength and stiffness deterioration." *Earthquake Engineering and Structural Dynamics*, 34(12).

Lignos, D. G. (2008). "Sidesway collapse of deteriorating structural systems under earthquake excitations." Ph.D. thesis, Department of Civil and Environmental Engineering, Stanford University, Stanford California.

Lignos, D. G. and Krawinkler, H. (2011). "Deterioration modeling of steel components in support of collapse prediction of steel moment frames under earthquake loading." *ASCE Journal of Structural Engineering*, 137(11), 1291–1302.

Mazzoni, S., McKenna, F., Scott, M. H., and Fenves, G. L. (2009). *The OpenSees command language manual, Version 2.0.* Pacific Earthquake Eng. Research Center, Univ. California at Berkeley.

Medina, R. and Krawinkler, H. (2005). "Evaluation of drift demands for the seismic performance assessment of frames." *ASCE Journal of Structural Engineering*, 131(7), 1003–1013.

Neuenhofer, A. and Filippou, F. (1997). "Evaluation of nonlinear frame finite-element models." *Journal of Structural Engineering*, 123(7), 958–966.

PEER/ATC (2010). "Modeling and acceptance criteria for seismic design and analysis of tall buildings." *Report No. 72-1*, ATC - Applied Techonology Council.

Pincheira, J., Dotiwala, F., and D'Souza, J. (1999). "Seismic analysis of older reinforced concrete columns." *Earthquake Spectra*, 15(2), 245–272.

Rahnama, M. and Krawinkler, H. (1993). "Effects of soft soil and hysteresis model on seismic demands." *John A. Blume Earthquake Engineering Center Report*, (108).

Ribeiro, F. L., Barbosa, A. R., Scott, M. H., and Neves, L. C. (2014). "Deterioration modeling of steel moment resisting frames using finite-length plastic hinge force-based beam-column elements." *Journal of Structural Engineering*, 10.1061/(ASCE)ST.1943-541X.0001052.

Roufaiel, M. and Meyer, C. (1987). "Analytical modeling of hysteretic behavior of r/c frames." *ASCE Journal of Structural Engineering*, 113(3), 429–444.

Scott, M. H. and Fenves, G. L. (2006). "Plastic hinge integration methods for force-based beam-column elements." *ASCE Journal of Structural Engineering*, 132(2), 244–252.

Scott, M. H. and Fenves, G. L. (2010). "Krylov subspace accelerated newton algorithm: Application to dynamic progressive collapse simulation of frames." *ASCE Journal of Structural Engineering*, 136(5), 473–480.

Scott, M. H. and Ryan, K. L. (2013). "Moment-rotation behavior of force-based plastic hinge elements." *Earthquake Spectra*, 29(2), 597–607.

Sivaselvan, M. and Reinhorn, A. (2000). "Hysteretic models for deteriorating inelastic structures." *ASCE Journal of Engineering Mechanics*, 126(6), 633–640.

Spacone, E., Filippou, F., and Taucer, F. (1996). "Fibre beam-column model for non-linear analysis of R/C frames: Part I. formulation." *Earthquake Engineering and Structural Dynamics*, 25(7), 711–726.

Takeda, T., Sozen, M., and Nielson, N. (1970). "Reinforced concrete response to simulated earthquakes." *ASCE Journal of the Structural Division*, 96(12), 2557–2573.

Zareian, F. and Medina, R. A. (2010). "A practical method for proper modeling of structural damping in inelastic plane structural systems." *Computers & Structures*, 88(1-2), 45–53.

List of Tables

TABLE 1. ModIMK model parameters used in the numerical examples

Model	EI (kN.m^2)	$M_y^+ and M_y^-$ (kN.m)	M_c/M_y	θ_p (rad)	θ_{pc} (rad)	κ	$E_t^{M-\theta}$ (kN.m)
All models	2.33×10^6	1911	1.05	0.233	0.156	0.4	2255

List of Figures

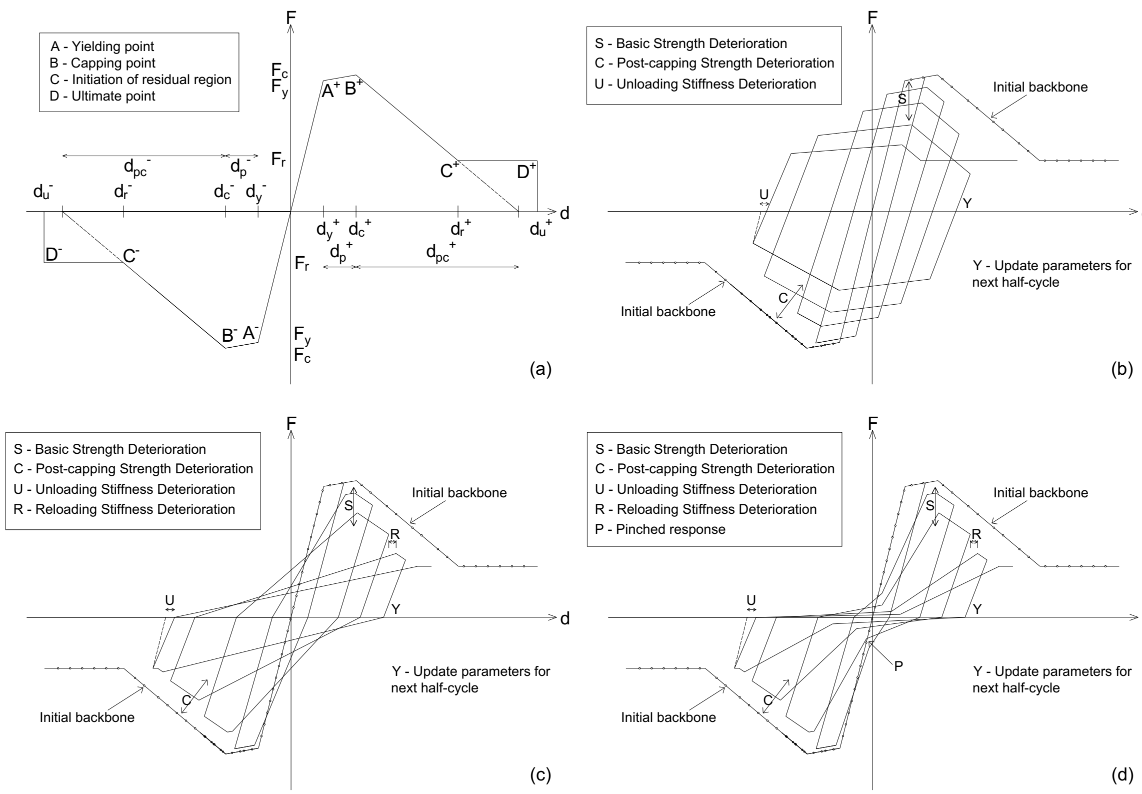

FIG. 1. Modified Ibarra-Medina-Krawinkler deterioration models: (a) backbone curve, (b) Bilin model, (c) Peak-oriented model, and (d) Pinching model.

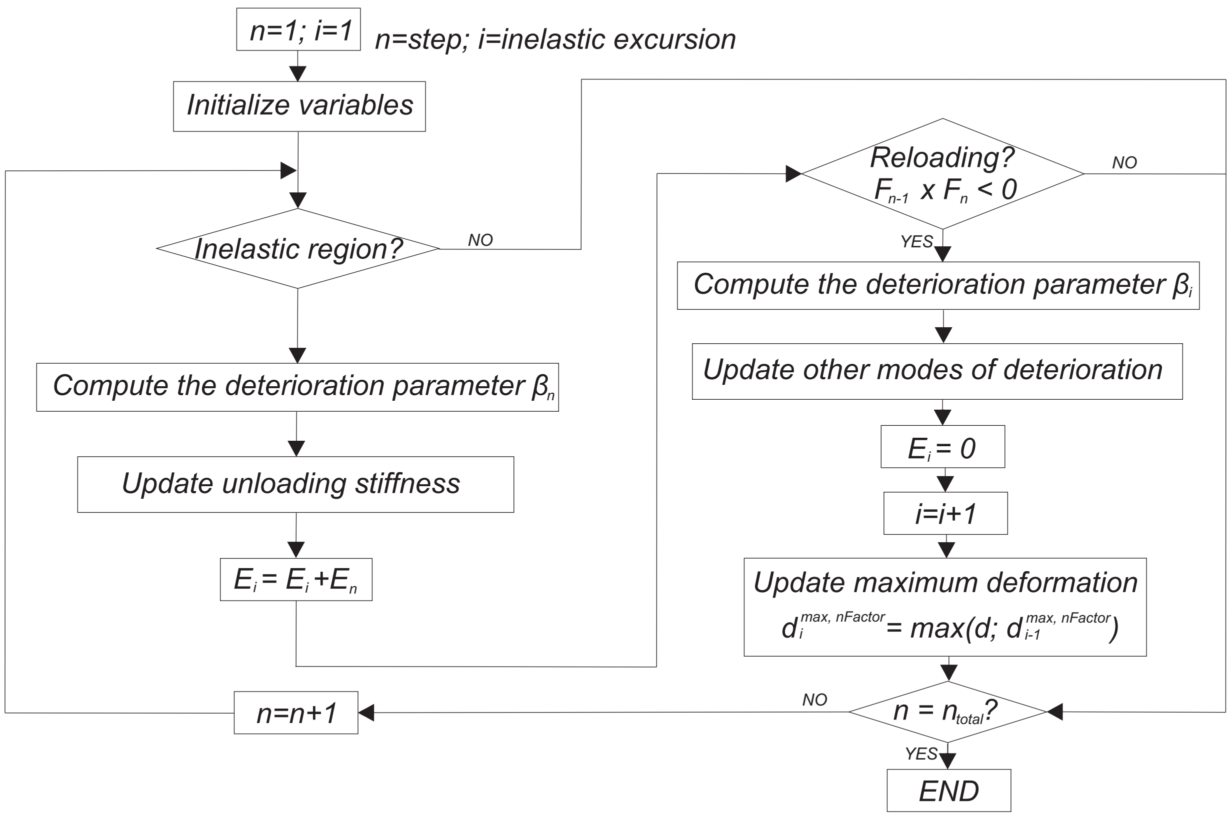

FIG. 2. General procedure for updating model parameters during cyclic analysis

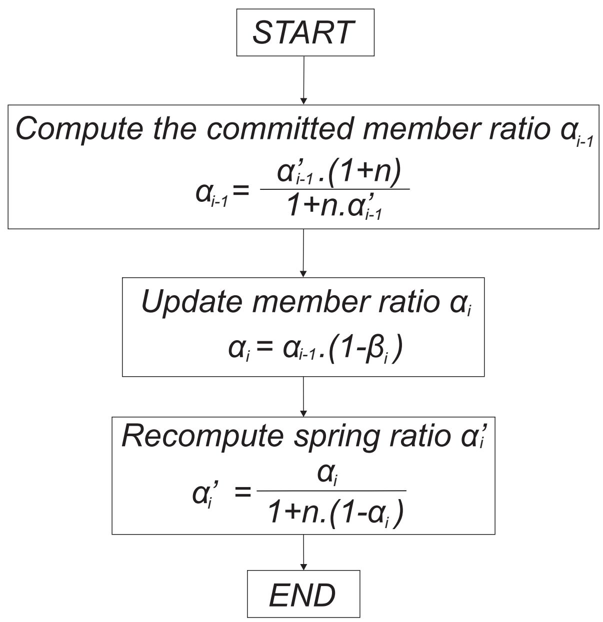

FIG. 3. Procedure for updating post-yielding ratio during cyclic analysis for Concentrated Plasticity Hinge model

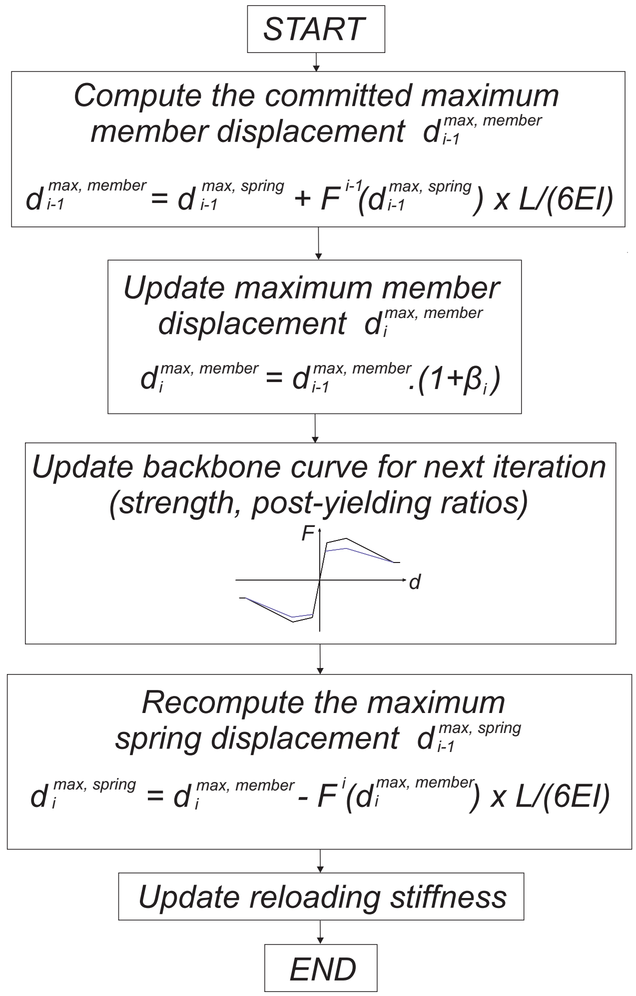

FIG. 4. Procedure for updating reloading stiffness during cyclic analysis for Concentrated Plasticity Hinge model

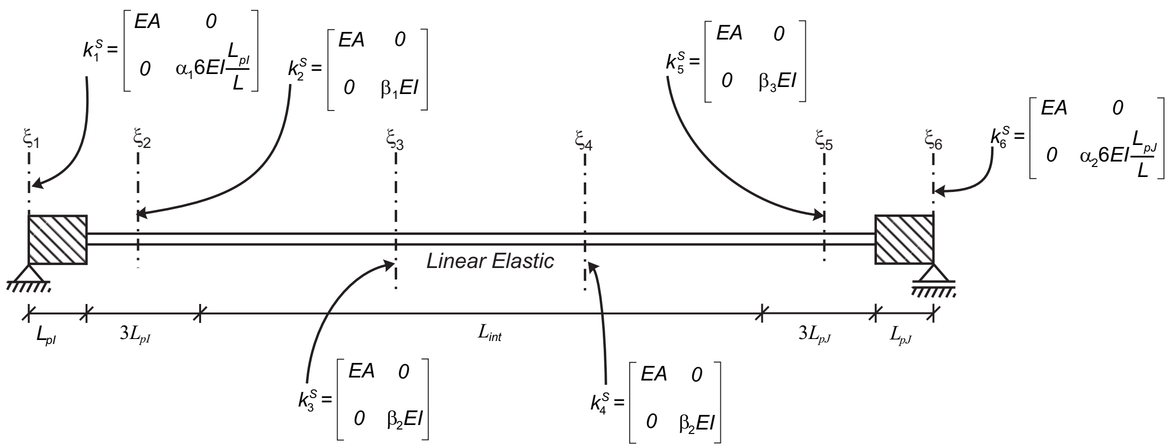

FIG. 5. Modified Gauss-Radau integration scheme considering flexural stiffness modification parameters (β_1, β_2 and β_3)

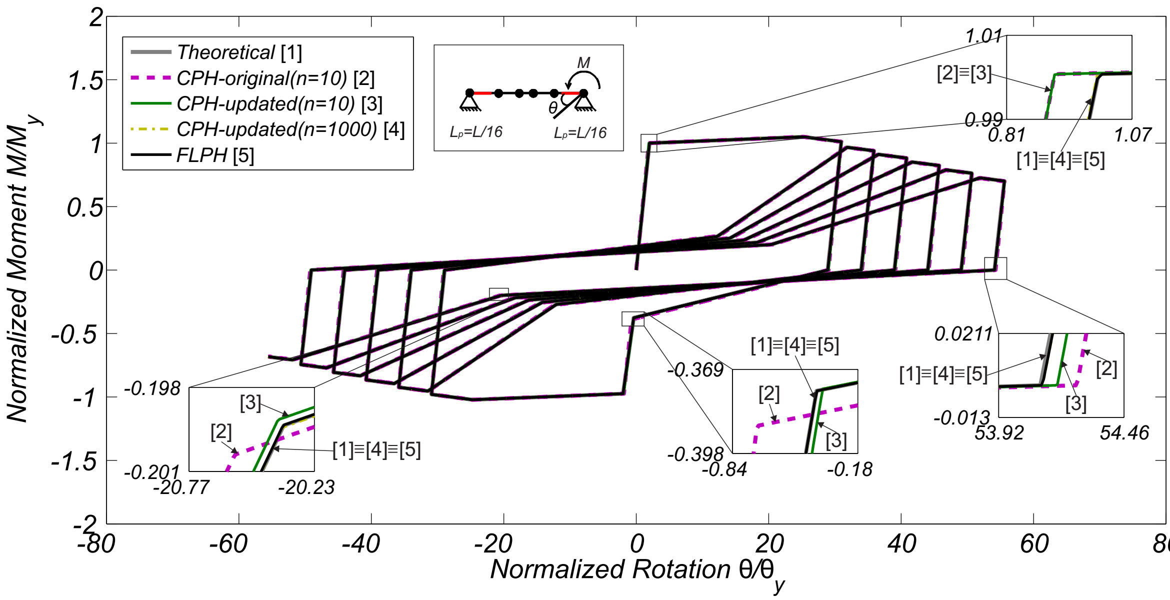

FIG. 6. Pinching model - cyclic analysis considering a single end moment

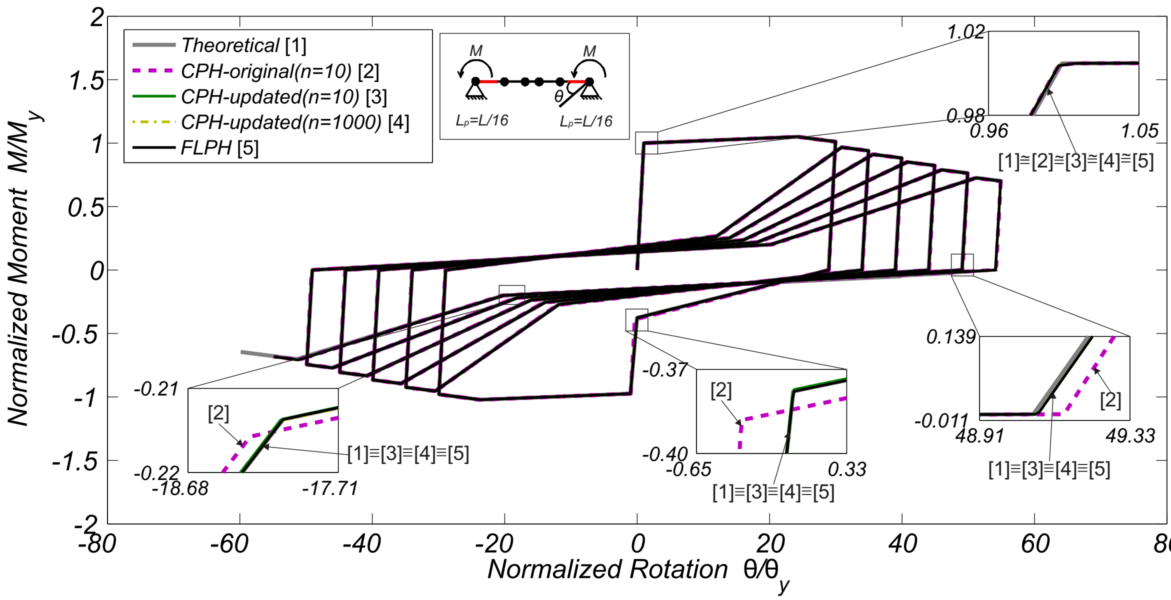

FIG. 7. Pinching model - cyclic analysis considering anti-symmetric end moments

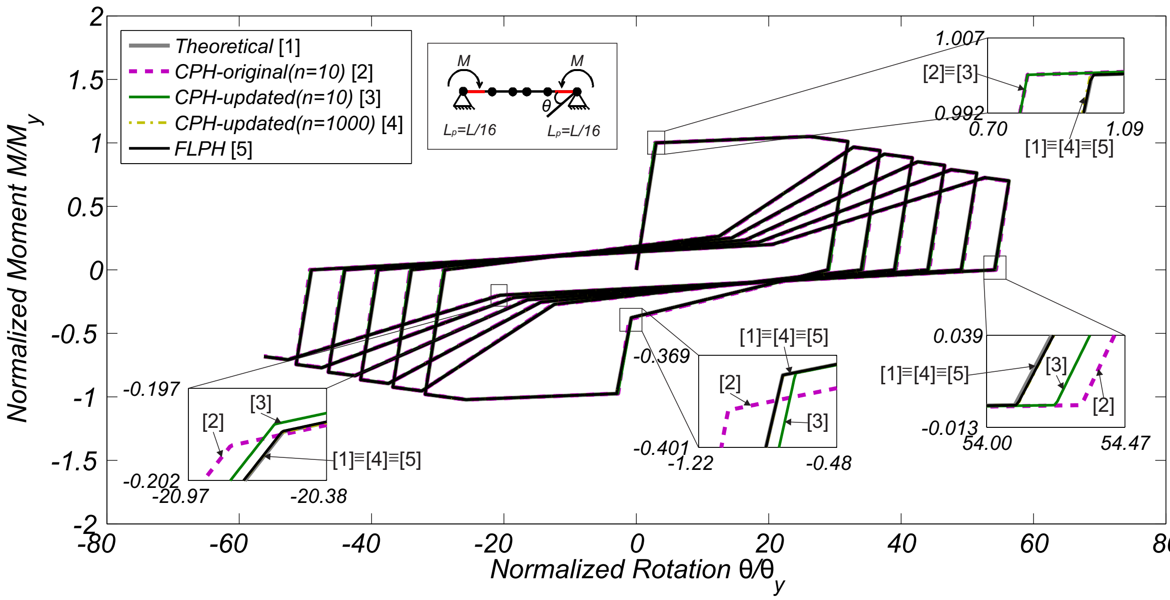

FIG. 8. Pinching model - cyclic analysis considering symmetric end moments

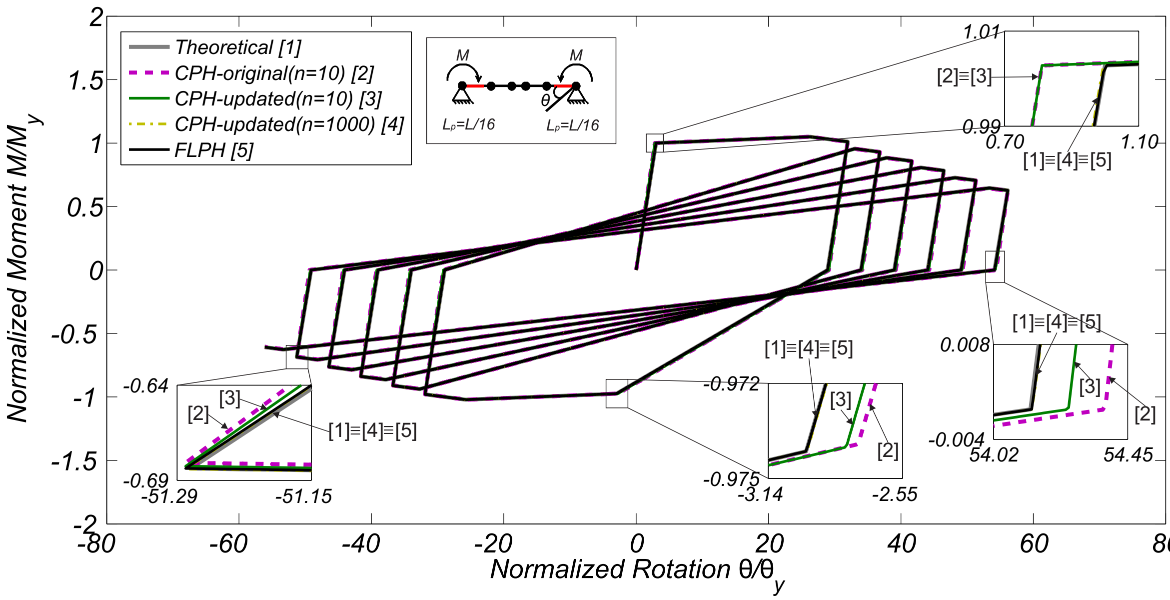

FIG. 9. Peak-oriented model - cyclic analysis considering symmetric end moments

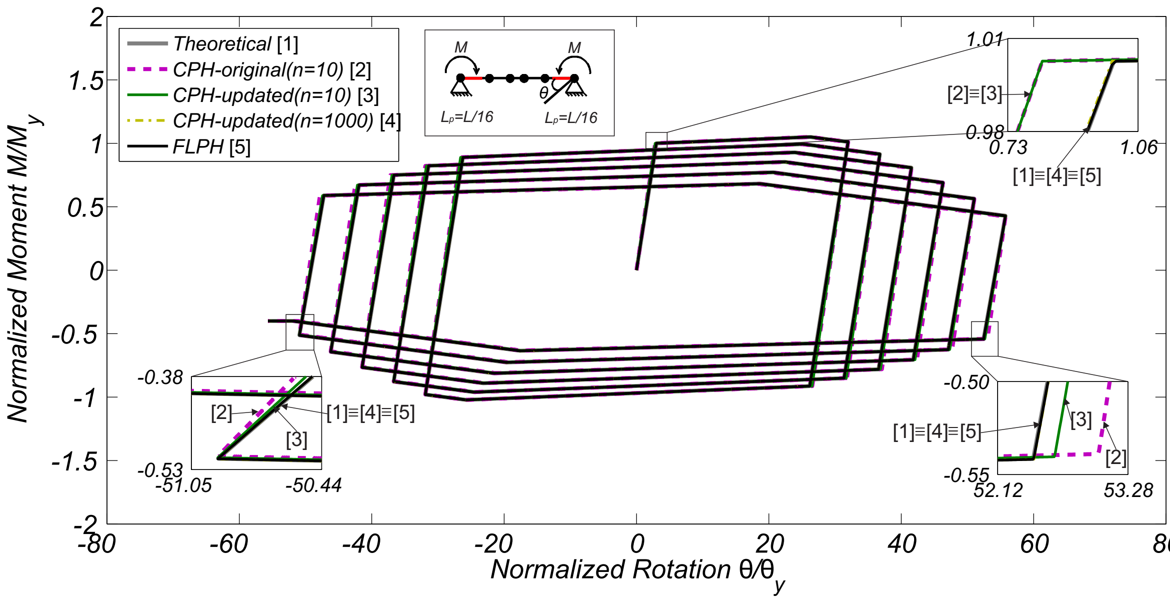

FIG. 10. Bilin model - cyclic analysis considering symmetric end moments

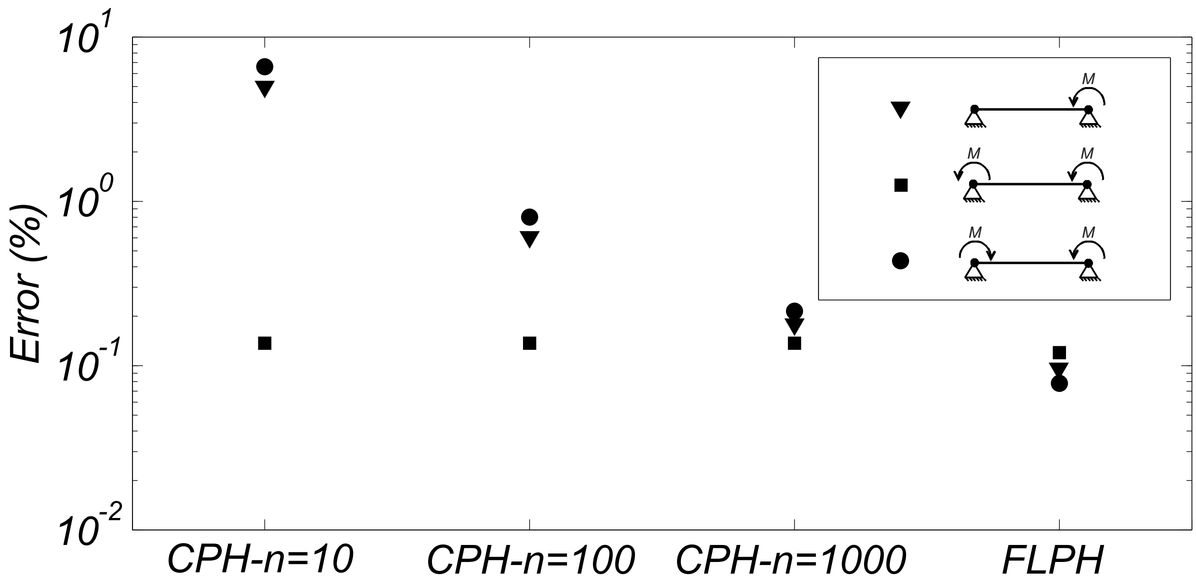

FIG. 11. Comparison of error in the elastic stiffness for CPH-updated with different values of n_{Factor} and FLPH

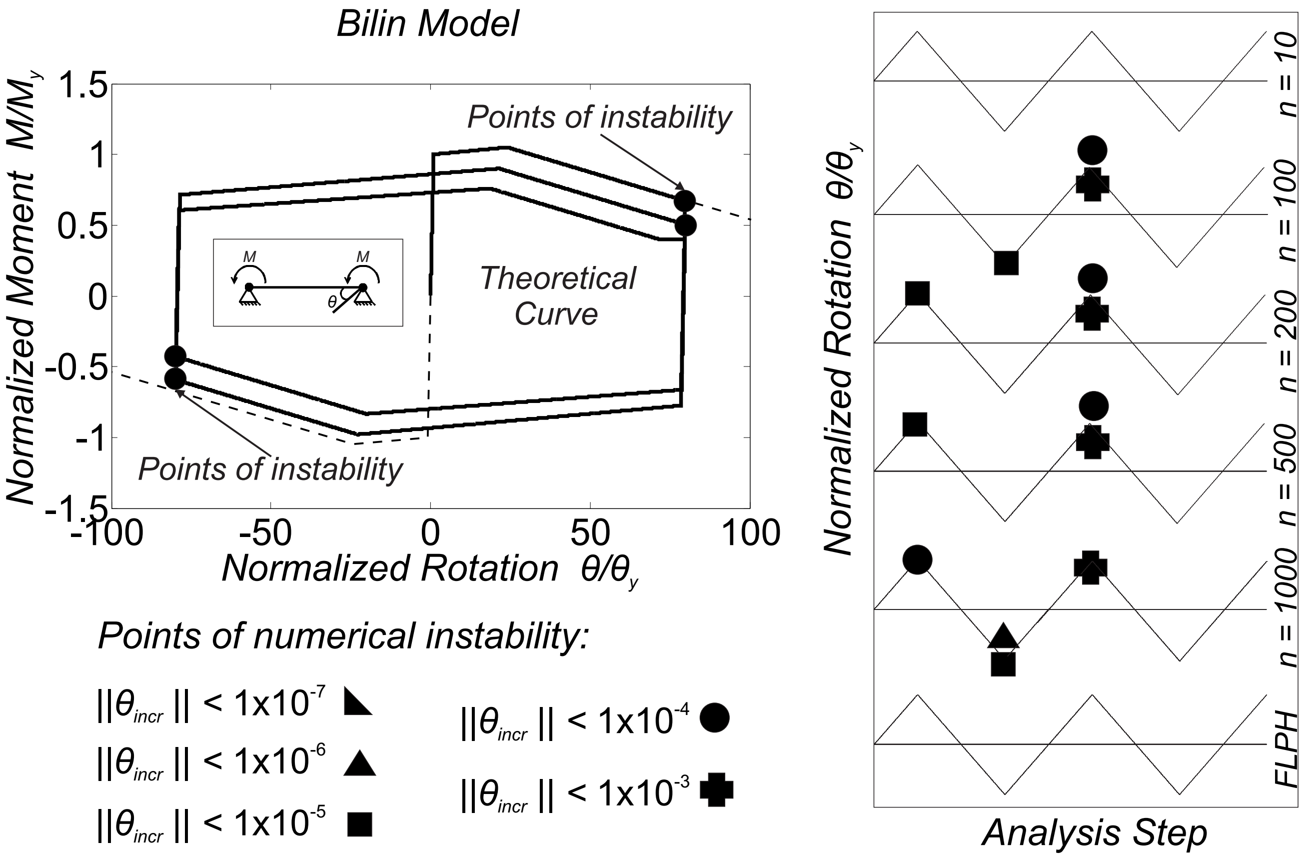

FIG. 12. Convergence stability analysis using the Bilin model